Article

Adsorption and Sensing Properties of Ni-Modified InSe Monolayer Towards Toxic Gases: A DFT Study

Jianhong Dong [1], Xiaoqian Qiu [1], Shuying Huang [1], Shaomin Lin [1,*], Lisha Liu [2] and Huihui Xiong [3,*]

1　School of Materials Science and Engineering, Hanshan Normal University, Chaozhou 521041, China; dongjh@hstc.edu.cn (J.D.); 202201017203@stu.hstc.edu.cn (X.Q.); 202301017232@stu.hstc.edu.cn (S.H.)
2　College of Arts, Hanshan Normal University, Chaozhou 521041, China; 8151@hstc.edu.cn
3　School of Metallurgy Engineering, Jiangxi University of Science and Technology, Ganzhou 341000, China
*　Correspondence: lsm678@hstc.edu.cn (S.L.); xionghui8888@126.com (H.X.)

Abstract: The emission of toxic gases from industrial production has intensified issues related to atmospheric pollution and human health. Consequently, the effective real-time monitoring and removal of these harmful gases have emerged as significant challenges. In this work, the density functional theory (DFT) method was utilized to examine the adsorption behaviors and electronic properties of the Ni-decorated InSe (Ni-InSe) monolayer when interacting with twelve gases (CO, NO, NO_2, NH_3, SO_2, H_2S, H_2O, CO_2, CH_4, H_2, O_2, and N_2). A comparative assessment of adsorption strength and sensing properties was performed through analyses of the electronic structure, work function, and recovery time. The results show that Ni doping enhances the electrical conductivity of the InSe monolayer and improves the adsorption capabilities for six toxic gases (CO, NO, NO_2, NH_3, SO_2, and H_2S). Furthermore, the adsorption of these gases on the Ni-InSe surface is characterized as chemisorption, as indicated by the analysis of the adsorption energy, density of states, and charge density difference. Additionally, the adsorption of CO, NO, NO_2, and SO_2 results in significant alterations to the bandgap of Ni-InSe, with changes of 18.65%, 11.37%, 10.62%, and −31.77%, respectively, underscoring its exceptional sensitivity. Moreover, the Ni-InSe monolayer exhibits a moderate recovery time of 3.24 s at 298 K for the SO_2. Consequently, the Ni-InSe is regarded as a promising gas sensor for detecting SO_2 at room temperature. This research establishes a foundation for the development of an Ni-InSe-based gas sensor for detecting and mitigating harmful gas emissions.

Keywords: doped InSe monolayer; gas sensor; DFT method; adsorption mechanism

1. Introduction

The detection of toxic gases such as carbon monoxide (CO), nitric oxide (NO), nitrogen dioxide (NO_2), ammonia (NH_3), sulfur dioxide (SO_2), and hydrogen sulfide (H_2S) is of paramount importance due to their detrimental effects on both human health and the environment [1,2]. These gases are common pollutants originating from various industrial activities, vehicular emissions, and agricultural practices [3]. In response to this pressing issue, researchers have continually sought advanced materials and methodologies to improve gas-sensing technologies. Traditional gas-sensing materials often face challenges in terms of sensitivity, selectivity, and response time. Therefore, the exploration of new materials is crucial for the development of advanced gas sensors capable of detecting low concentrations of toxic gases with high accuracy. Nowadays, two-dimensional (2D) materials, such as graphene [4], transition metal dichalcogenides (TMDs) [5,6], $MoSi_2N_4$ [7], metal oxide [8], and phthalocyanine [9], have gained significant attention due to their unique properties, high surface area, and tunable electronic structure [10–12], which make them promising candidates for highly sensitive and selective gas sensors [13].

Among these materials, the 2D InSe has emerged as a promising candidate for gas-sensing applications [14]. The InSe monolayer is a layered material with a van der Waals

structure, allowing for the easy exfoliation into thin layers with large surface areas. This structural feature enhances the adsorption of gas molecules onto the InSe surface, facilitating interaction and detection at the molecular level [15]. Additionally, InSe exhibits tunable electronic properties, enabling the modulation of its conductivity in the presence of different gases through charge transfer mechanisms [16]. In recent years, there has been a growing interest in exploring the gas-sensing properties of 2D materials using density functional theory (DFT) calculations [17]. For example, Cai et al. [14] and Ma et al. [18] utilized the DFT method to investigate the adsorption behaviors and sensing properties of the InSe monolayer to CO, NO, NO_2, H_2S, and NH_3, and found that the InSe monolayer was sensitive to NO and NO_2. Nevertheless, the InSe monolayer exhibits a poor capture ability towards these toxic gases due to the weak physisorption, which hinders its practical applications. Fortunately, there are several innovative strategies to enhance the performance of InSe-based gas sensors, including atomic doping [19], surface functionalization [20], defect engineering [21], and the design of heterostructures [22,23]. Among them, the transition metal (TM) doping is regarded as an effective method to improve the sensitivity and selectivity. For instance, the Ru-modified InSe monolayer exhibits stable chemisorption and showcases a superior sensitivity for NH_3, NO_2, and SO_2 [24]. Moreover, the sensitivity of the InSe monolayer to the CO_2 molecule can be enhanced after the doping of Pt, Ag, Au, and Pd atoms [25].

In addition to these noble metal atoms [26,27], the incorporation of affordable nickel atoms into 2D materials has also been extensively utilized in gas sensor applications. Initially, the nickel atoms in single-atom catalysts exhibit superior atomic efficiency, activity, and selectivity for gas-sensitive materials [28]. Furthermore, the electrical conductivity of the sensing materials can be regulated through nickel atom doping, enhancing the adsorption and sensing capabilities of the materials towards specific gases [29]. Consequently, the Ni-modified InSe (Ni-InSe) monolayer has a great potential to be a promising sensing material for toxic gases. In this work, the first-principle calculations are employed to explore the adsorption mechanism and sensing performance of the InSe monolayer towards 12 kinds of gases (CO, NO, NO_2, NH_3, SO_2, H_2S, H_2O, CO_2, CH_4, H_2, O_2, and N_2). Firstly, the investigation focuses on the potential stable adsorption of twelve gases on the Ni-InSe surface through the analyses of the geometrical optimization, adsorption energy, charge density difference, and density of states. Then, the sensing properties of the InSe monolayer to the target toxic gases are evaluated by analyzing the changes in conductivity, work function, and recovery time before and after gas adsorption. In conclusion, this study aims to provide theoretical guidance for achieving the online monitoring of Ni-InSe-based gas sensors to these toxic gases.

2. Computational Method and Details

In this work, all DFT simulations were carried out using the DMol^3 package within the Materials Studio 2020 software [30]. The Perdew–Burke–Ernzerhof (PBE) functional, which belongs to the generalized gradient approximation (GGA) family [31], was employed to handle the electron exchange and correlation effects. Given that PBE has limitations in accurately describing dispersion interactions, a density functional theory correction for dispersion (DFT-D) was incorporated to address this shortfall. Specifically, the Grimme method [31] was utilized for van der Waals force corrections. To further improve the calculation precision, the double numerical polarization (DNP) basis set [32] along with DFT semi-core pseudopotentials (DSSPs) [33] was used. For the Brillouin zone integration [34], a $7 \times 7 \times 1$ k-point grid combined with a $4 \times 4 \times 1$ supercell was employed to ensure sufficient segmentation accuracy. A vacuum layer of 20 Å was inserted into the computational model to prevent interactions between periodic images. The energy convergence threshold was set to 1.0×10^{-5} Ha, while the maximum force was constrained to 0.002 Ha/Å, and the maximum displacement was limited to 0.005 Å. The self-consistent field (SCF) calculations were subject to a charge density convergence criterion of

1.0×10^{-6} Ha. Furthermore, a real-space global orbital cutoff radius of 5.0 Å combined with a Gaussian smearing parameter of 0.005 Ha was implemented.

The binding energy (E_{bin}) can be utilized to evaluate the stability of the Ni-InSe monolayer, which can be determined by the following [35]:

$$E_{\text{bin}} = E_{\text{Ni-InSe}} - E_{\text{InSe}} - E_{\text{Ni}} \tag{1}$$

where the $E_{\text{Ni-InSe}}$, E_{InSe}, and E_{Ni} are the total energies of Ni-InSe, pristine InSe, and a single Ni atom, respectively. To access the interaction strength between the gases and InSe monolayer, the adsorption energy (E_{ads}) of each system can be calculated by the following [36]:

$$E_{\text{ads}} = E_{\text{gas/Ni-InSe}} - E_{\text{Ni-InSe}} - E_{\text{gas}} \tag{2}$$

In this equation, the $E_{\text{gas/Ni-InSe}}$, $E_{\text{Ni-InSe}}$, and E_{gas} are the total energies of gas adsorbed on Ni-InSe, clean Ni-InSe, and an isolated gas molecule, respectively. Moreover, the adsorption strength of Ni-InSe towards the target gases can be also evaluated by the charge transfer (Q_{T}), which can be obtained by the following equation [37,38]:

$$Q_{\text{T}} = Q_{\text{adsorbed-gas}} - Q_{\text{isolated-gas}} \tag{3}$$

where the $Q_{\text{adsorbed-gas}}$ and $Q_{\text{isolated-gas}}$ represent the charge number of adsorbed gas and isolated gas, respectively. The negative Q_{T} implies that the adsorbed gas gains electrons from the Ni-InSe monolayer, while the positive Q_{T} means that the adsorbed gas loses some electrons transferring to the Ni-InSe monolayer.

3. Results and Discussion

3.1. Structural and Electronic Properties of Ni-InSe Monolayer

The crystal structure of 2D InSe is a layered hexagonal lattice, with each layer consisting of indium and selenium atoms arranged in a honeycomb pattern. The calculated lattice constant of the pristine InSe is approximately 4.07 Å with a space group of P-6m2. As shown in Figure 1a, the $4 \times 4 \times 1$ supercell encompasses 32 In atoms and 32 Se atoms, with respective bond lengths of 2.804 Å and 2.676 Å for the In-In and In-Se bonds. These parameters match well with the previously reported results. The band structure and partial density of state (PDOS) of the InSe monolayer are depicted in Figure 1b,c. Notably, the single-layer InSe exhibits a semiconductor characteristic with an indirect bandgap of 1.968 eV, which is consistent with the reported data (2.02 eV) [15,39] and experimental result [40]. From Figure 1c, obvious hybridizations can be observed between Se-p and In-p, and d orbitals in the energy ranging from −6.00 eV to the Fermi level. Moreover, the s, p, and d orbitals of the In atom also overlap with the Se-s orbital, and there exists a significant resonance peak at about −14.30 eV due to the hybridization between the Se-d and In-d orbitals. This indicates that the strong In-Se covalent bond is formed, and, thus, the InSe possesses excellent stability.

To explore the most stable Ni-InSe monolayer, different doping sites, including the bridge site, Setop site, Intop site, and hollow site, are considered for the Ni atom (Figure 1a). Following full relaxation, the largest binding energy occurs at the hollow site (−3.81 eV), followed by the bridge site (−3.76 eV), the Intop site (−3.25 eV), and the Setop site (−1.83 eV). Thus, the Ni atom is preferentially adsorbed on the hollow site, as depicted in Figure 2a. Moreover, it can be seen from Figure 2b that the introduction of the Ni atom causes the conduction band minimum (CBM) to shift towards the Fermi level, leading to a reduction in the bandgap from 1.968 eV to 1.196 eV. This indicates that Ni doping enhances the electrical conductivity of the InSe monolayer and is beneficial for improving its gas-sensitive properties. Additionally, as displayed in the PDOS of Ni-InSe (Figure 2c), the Ni-d orbital strongly interacts with the Se-p, In-p, and d orbitals within the energy of −7.00 eV to 2.50 eV, with several resonance peaks observed at approximately −6.00 eV, −3.08 eV, −0.15 eV, and 1.52 eV. Moreover, the Ni-p orbital also overlaps with the Se-d and

In-s orbital in the whole energy range. As a result, two robust Ni-Se and Ni-In bonds are formed within the Ni-InSe monolayer. The stability of Ni-InSe is further assessed through an ab initio molecular dynamic (AIMD) simulation at 398 K, as shown in Figure 3. The temperature and potential energy of Ni-InSe display minimal fluctuations during the time of 10 ps, with no discernible disruption of existing bonding within the material. Thus, the Ni-InSe monolayer exhibits exceptional stability and holds promise as a highly efficient sensing material.
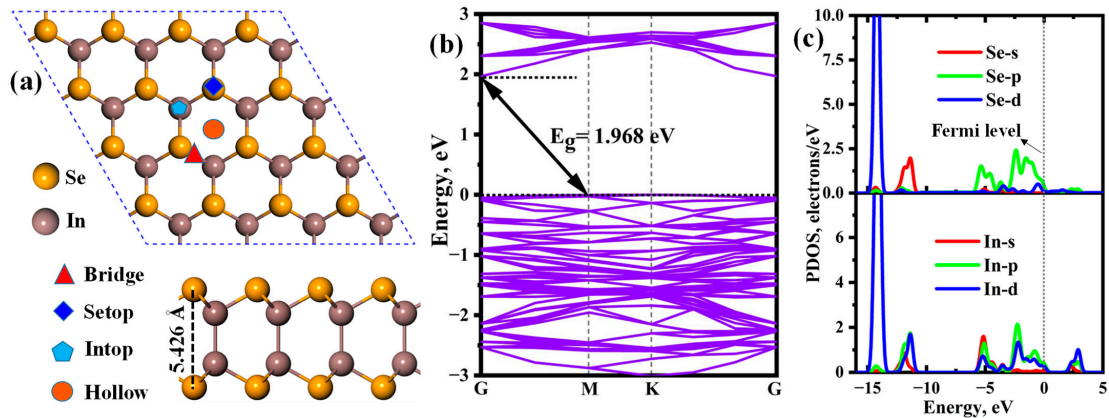

Figure 1. (**a**) Top and side views of geometrical configuration, (**b**) band structure and (**c**) partial density of state (PDOS) of the InSe monolayer. Reprinted with the permission from Ref. [41]. Copyright 2024 Elsevier.
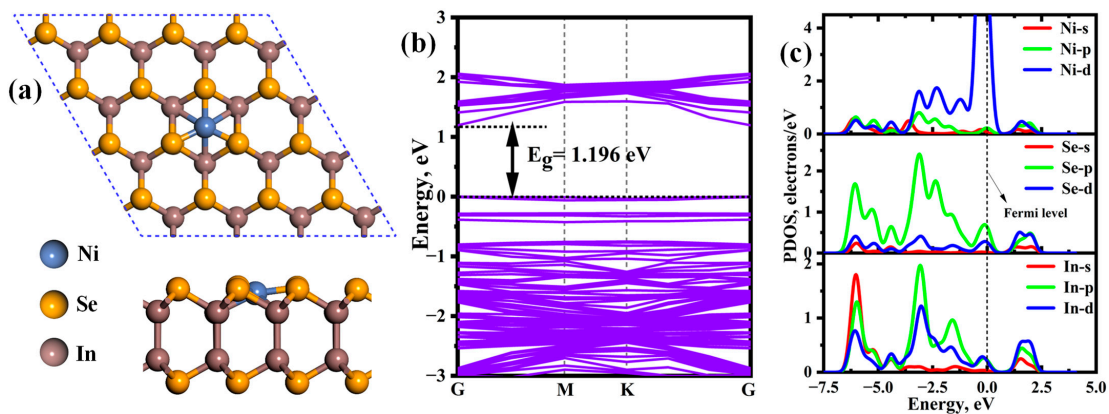

Figure 2. (**a**) Top and side views of geometrical configuration, (**b**) band structure and (**c**) partial density of state (PDOS) of the In-doped InSe monolayer.
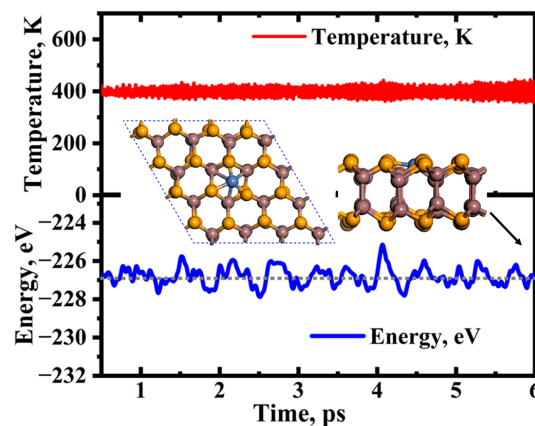

Figure 3. Molecular dynamics simulations of Ni-InSe monolayer at 398 K.

3.2. Adsorption of Different Gases on Ni-InSe Monolayer

This section discusses the adsorption characteristics of 12 different gases on the surface of Ni-InSe. During the simulation process, only the Ni atom is considered as the active site and different adsorption orientations of these gases have been taken into account. Through a comparison, the most stable configuration of each adsorption system has been ascertained, and its adsorption parameters are shown in Table 1. It is observed that six toxic gases (CO, NO, NO_2, NH_3, SO_2, and H_2S) exhibit relatively high adsorption energy values of -0.74 eV to -1.35 eV, with adsorption distances ranging from 1.663 Å to 2.243 Å. As shown in Figure 4, CO, NO, and H_2S are adsorbed on the Ni-InSe monolayer with a small dip angle, while NO_2, NH_3, and SO_2 are perpendicularly adsorbed on the Ni-InSe surface. Evidently, the adsorption distances of these six noxious gases are all less than their respective R_{sum}, indicating the formation of chemical bonds in those adsorption systems. Hence, these noxious gases are interpreted as undergoing chemical adsorption, wherein CO, NO, NH_3, and H_2S donate a certain number of electrons to the Ni-InSe and act electron donators, while NO_2 and SO_2 gain 0.223 e and 0.040 e from the Ni-InSe monolayer, respectively, and thus act as electron acceptors.

Table 1. Adsorption parameters, bandgap (E_g) and work function (Φ) of different gases adsorbed on Ni-InSe monolayer. D and R_{sum} are the adsorption distance and the theoretical sum of radii of two atoms.

Gas Molecules	E_{ads}	Q_T, e	D, Å	R_{sum}, Å	E_g, eV	Φ, eV
CO	-1.35	0.164	1.777 (Ni−C)	2.44 (Ni−C)	1.419	5.66
NO	-1.26	0.082	1.663 (Ni−N)	2.33 (Ni−N)	1.323	5.578
NO_2	-0.94	-0.223	1.926 (Ni−N)	2.33 (Ni−N)	0.816	5.361
NH_3	-0.95	0.246	2.106 (Ni−N)	2.33 (Ni−N)	1.142	4.844
SO_2	-0.74	-0.040	2.086 (Ni−S)	2.65 (Ni−S)	1.332	5.905
H_2S	-0.79	0.235	2.243 (Ni−S)	2.65 (Ni−S)	1.190	5.061
H_2O	-0.48	0.123	2.311 (Ni−O)	2.25 (Ni−O)	1.163	5.007
CO_2	-0.18	0.016	3.492 (Ni−C)	2.44 (Ni−C)	1.201	5.306
CH_4	-0.20	0.029	3.320 (Ni−C)	2.44 (Ni−C)	1.195	5.279
H_2	-0.13	0.014	2.690 (Ni−H)	2.30 (Ni−H)	1.202	5.306
N_2	-0.56	0.071	1.828 (Ni−N)	2.33 (Ni−N)	1.400	5.578
O_2	-0.01	-0.007	2.354 (Ni−O)	2.25 (Ni−O)	1.197	5.311

3.3. Electronic Properties of Different Adsorption Systems

To further reveal the microscopic bonding mechanism between the Ni-InSe and toxic gases, the total electron density (TED) and charge density difference (CDD) of the Ni-InSe monolayer adsorbing CO, NO, NO_2, NH_3, SO_2, and H_2S are calculated, and the corresponding results are detailed in Figures 5 and 6. It can be seen that abundant electrons accumulate in the spaces between the toxic gases and Ni-InSe monolayer, as depicted by Figure 5a–f, illustrating that these gases and Ni-InSe share massive electrons, and, thus, strong interactions occur between them. Additionally, as shown in the CDD plots of Figure 6, the charge redistribution can be observed in the six adsorption systems after full relaxation. It is obvious that a large number of charges are gathered between the gases and the Ni-InSe monolayer, indicating their strong interactions. In particular, conspicuous electron-depleted regions are distributed around CO, NO, NH_3, and H_2S, and the electron-depleted regions of NH_3 and H_2S are larger than those of CO and NO, as illustrated by the blue areas in Figure 6a,b,d,f. Conversely, the electron accumulation regions gather around the Ni atoms of Ni-InSe. Consequently, CO, NO, NH_3, and H_2S donate 0.164 e, 0.082 e, 0.246 e, and 0.235 e to the Ni-InSe monolayer. By contrast, for the NO_2 and SO_2 adsorption systems, as shown in Figure 6c,e, a large number of electrons are accumulated around NO_2 and SO_2, with significant electron depletion regions appearing on the Ni-InSe surface. Thus, the Ni-InSe monolayer gain approximately 0.223 e and 0.04 e from the NO_2 and SO_2, respectively, and functions as an electron acceptor. In conclusion, the analyses

of both TED and CDD plots suggest that the six toxic gases strongly interact with Ni-InSe through chemical adsorption.
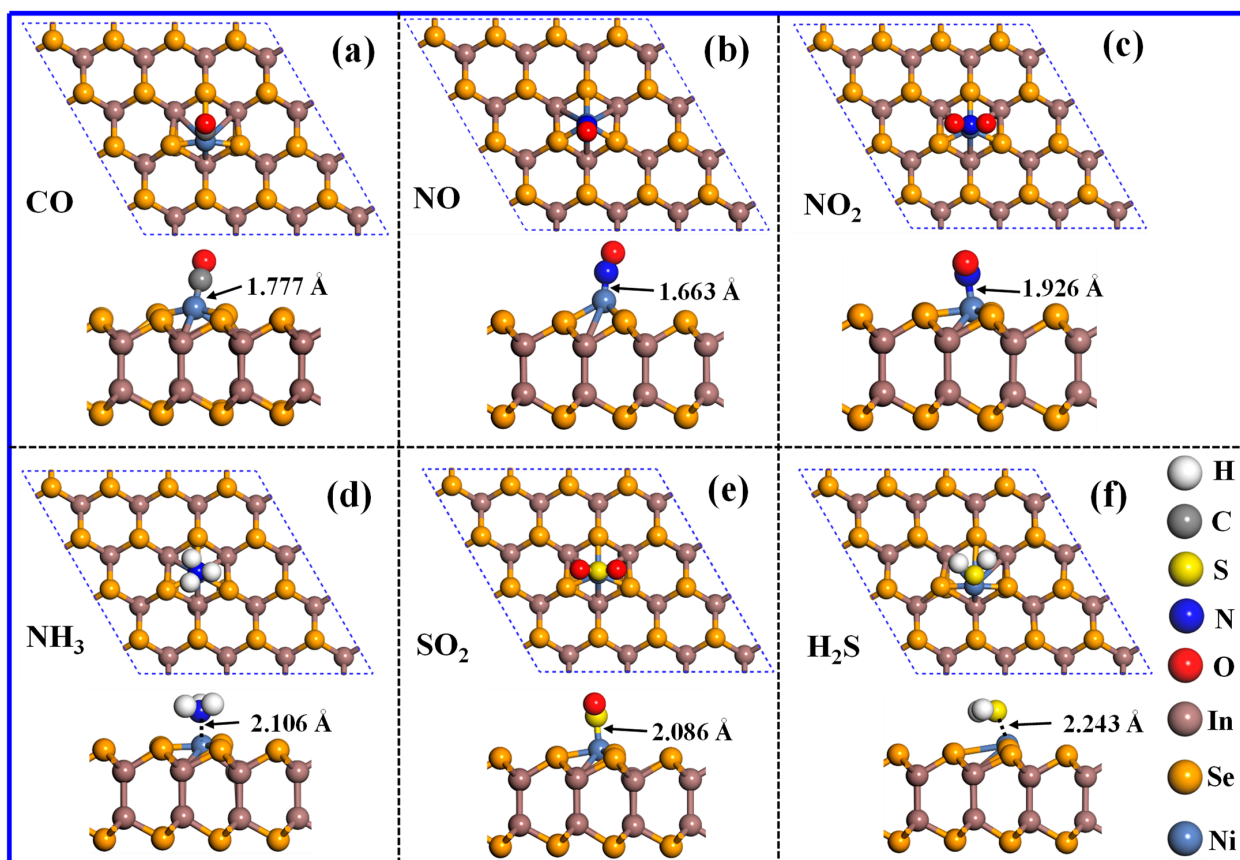

Figure 4. Atomic configurations of different adsorption systems: (**a**) CO/Ni-InSe, (**b**) NO/Ni-InSe, (**c**) NO_2/Ni-InSe, (**d**) NH_3/Ni-InSe, (**e**) SO_2/Ni-InSe, and (**f**) H_2S/Ni-InSe.
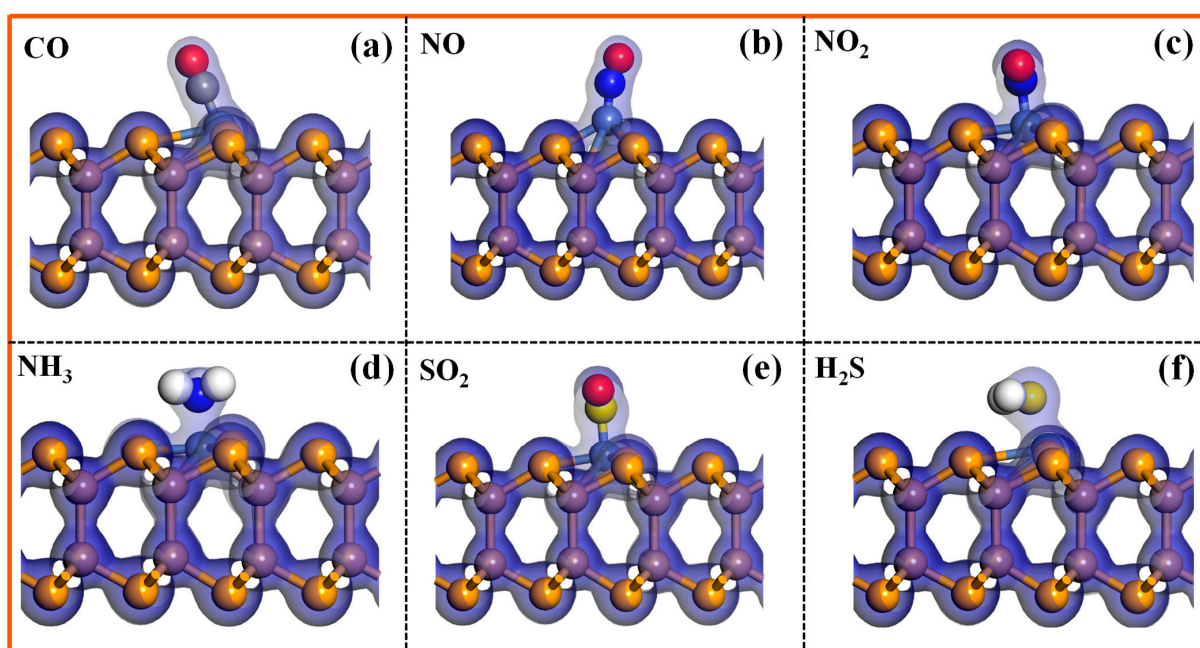
Figure 5. Total electron density (TED) of different adsorption systems: (**a**) CO/Ni-InSe, (**b**) NO/Ni-InSe, (**c**) NO_2/Ni-InSe, (**d**) NH_3/Ni-InSe, (**e**) SO_2/Ni-InSe, and (**f**) H_2S/Ni-InSe. The iso-value of TED is 0.2 e/Å^3.
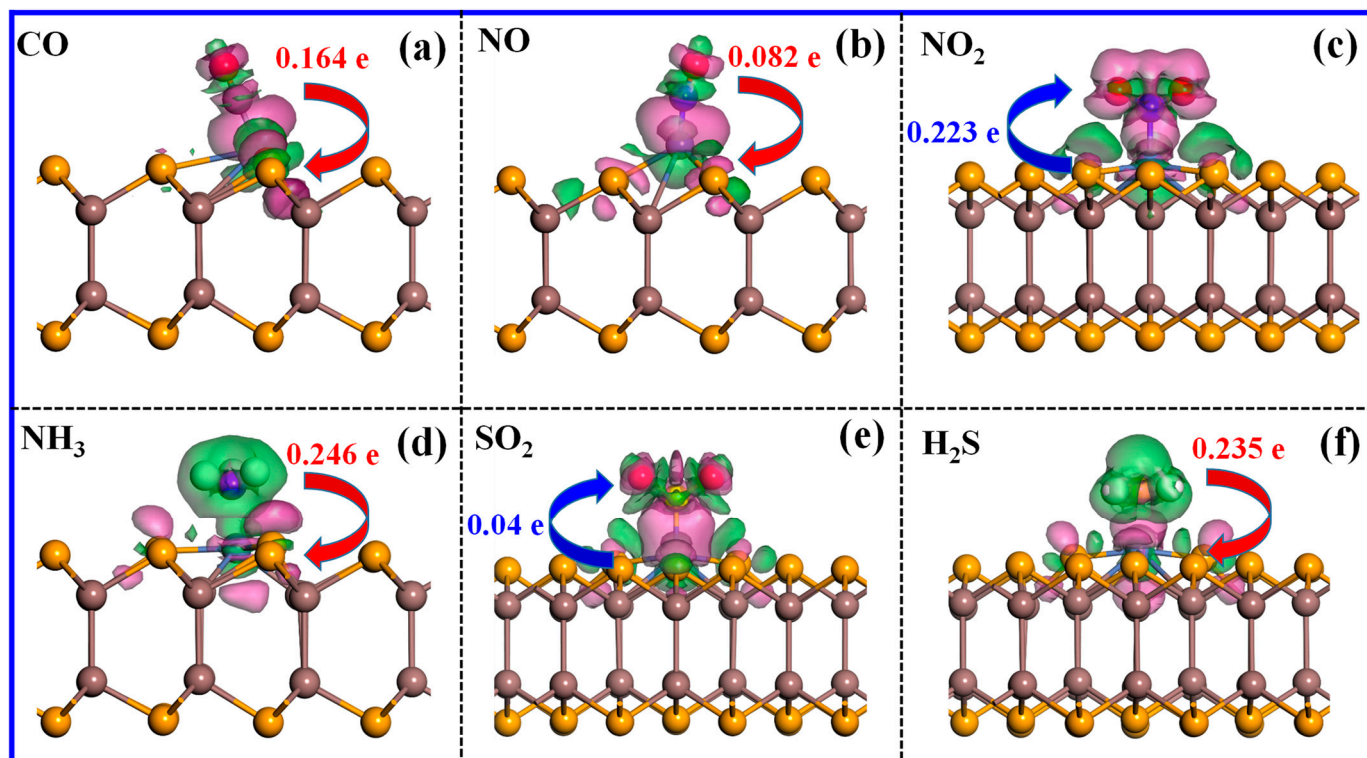
Figure 6. Charge density difference (CDD) of different adsorption systems: (**a**) CO/Ni-InSe, (**b**) NO/Ni-InSe, (**c**) NO_2/Ni-InSe, (**d**) NH_3/Ni-InSe, (**e**) SO_2/Ni-InSe, and (**f**) H_2S/Ni-InSe. The iso-value of CDD is ± 0.005 e/Å^3; the pink and green regions represent the electron gains and losses, respectively.

Figure 7 presents the partial density of states (PDOSs) of different adsorption systems. For the CO adsorption system (Figure 7a), the strong affinity of Ni-InSe towards NO stems primarily from the hybridization between the C-p and Ni-d orbitals within the energy range of -13.00 eV to 2.75 eV, yielding several discernible resonance peaks at about -12.50 eV, -8.60 eV, -5.80 eV, and 2.20 eV. Additionally, the C-s orbital strongly hybridizes with the Ni-p orbital within the energy range of -10.00 eV to -5.00 eV, resulting in two significant resonance peaks at approximately -8.60 eV and -6.10 eV. Consequently, a strong Ni-C covalent bond is formed in the CO/Ni-InSe system. In the cases of the NO, NO_2, and NH_3 adsorption systems, as depicted in Figure 7b–d, a notable overlap is observed between the N-s, and p orbitals of the three gases and Ni-d orbitals within the energy range spanning from -15.00 eV to 2.00 eV. Moreover, the number of resonance peaks for the NO adsorption system exceeds those for the NO_2 and NH_3 adsorption systems. Consequently, Ni-InSe shows a stronger adsorption capability towards NO in comparison to NO_2 and NH_3. With regard to the SO_2 and H_2S adsorption systems, the robust adsorption affinity of Ni-InSe for these two gases is primarily attributed to the hybridization between the S-p and Ni-d orbitals. Conversely, the orbital overlap between N-s and Ni-s, and p is relatively limited at similar energy levels. Particularly, the SO_2 adsorption system (Figure 7e) displays four pronounced resonance peaks at -14.70 eV, -13.00 eV, -5.80 eV, and -3.05 eV, with comparable resonances also observed in the H_2S adsorption system. Thus, Ni-InSe exhibits comparable affinities for SO_2 and H_2S through chemisorption.
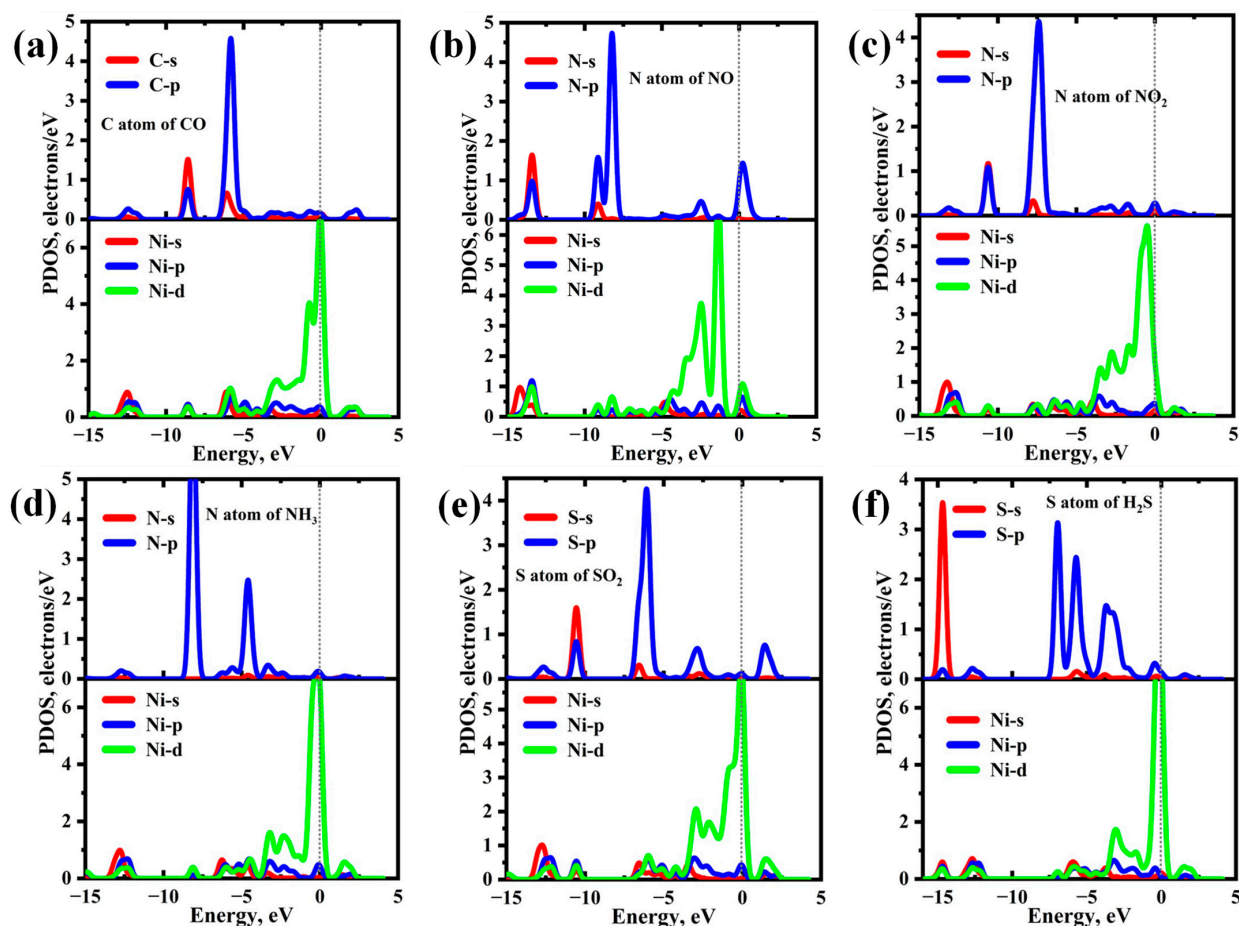
Figure 7. Partial density of states (PDOSs) of different adsorption systems: (**a**) CO/Ni-InSe, (**b**) NO/Ni-InSe, (**c**) NO_2/Ni-InSe, (**d**) NH_3/Ni-InSe, (**e**) SO_2/Ni-InSe, and (**f**) H_2S/Ni-InSe. The dashed lines represent the Fermi level.

3.4. Effect of H_2O on Adsorption

The emission of toxic gases usually occurs in humid atmospheres, making it crucial to study the impact of water molecules in the air. The most stable structure, PDOS, TED, and CDD of a single H_2O adsorbed on Ni-InSe monolayer are displayed in Figure 8. It is found that the Ni-InSe exhibits the weak adsorption strength of H_2O due to the small adsorption energy of -0.48 eV. And the H_2O is adsorbed on the top of the Ni atom with the adsorption distance of 2.311 Å, which is slightly smaller than the sum of the radii of Ni and O atoms (2.25 Å). Moreover, there are a few electrons shared between H_2O and Ni-InSe, as indicated by Figure 8d. Thus, the adsorption of H_2O belongs to physisorption and mainly interacts with the Ni-InSe monolayer through the van der Waals' force.

As shown in Figure 8e, the significant electron depletion region is accumulated around H_2O, while the electron accumulation region is primarily distributed on the Ni-InSe surface. Hence, about 0.123 e of H_2O is transferred to the Ni-InSe monolayer and the H_2O acts an electron donor, which agrees well with the above analysis of the Mulliken charge. From Figure 8c, the adsorption of H_2O is mainly ascribed by the hybridizations between O-p and Ni-s, p, and d orbitals in the energy level of -7.50 eV~2.50 eV, which results in three obvious resonance peaks at about -6.00 eV, -3.20 eV, and 0.00 eV. Furthermore, a significant orbital overlapping between O-s and Ni-s, p, and d orbitals can be observed at about -12.50 eV. However, these orbital hybridizations are not strong enough, and, thus, the adsorption of H_2O is relatively weak. As listed in Table 1, the adsorption strength of six toxic gases (CO, NO, NO_2, NH_3, SO_2, and H_2S) is much larger than that of the H_2O

molecule. Therefore, the existence of water in the air has no influence on the adsorption, capture, and even sensing properties of Ni-InSe towards these harmful gases.
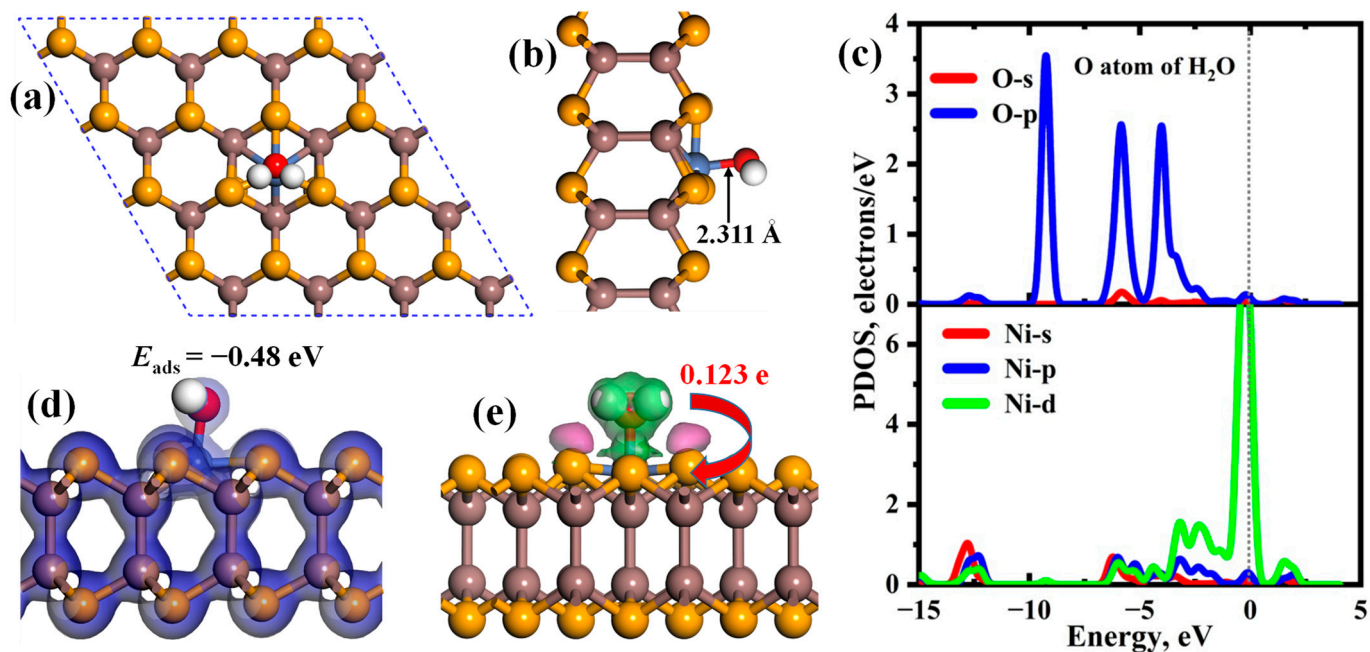

Figure 8. (**a**,**b**) Atomic structure, (**c**) PDOSs, (**d**) TED, and (**e**) CDD of a single H_2O adsorbed on Ni-InSe monolayer after full relaxation. The green and pink regions represent the charge depletion and charge accumulation, respectively.

3.5. Gas-Sensing Properties

The applicative efficacy and intrinsic value of gas sensors are intricately linked to their sensitivity, making it imperative to evaluate a sensing material's responsiveness to specific gases. The change in the electrical conductivity of gas-sensitive materials after gas adsorption determines the sensitivity of resistive gas sensors. The relationship between the electrical conductivity (σ) and band gap (E_g) can be described by the equation [3,42,43]:

$$\sigma = A \cdot \exp(-E_g/2K_B T) \tag{4}$$

where A, E_g, K_B, and T represent the constant, bandgap, Boltzmann constant, and temperature, respectively. Evidently, a smaller bandgap corresponds to a higher conductivity. A notable alteration in the electrical conductivity can elicit detectable electrical signals, thus facilitating the detection of the target gases. Therefore, if the change in the substrate's bandgap before and after gas adsorption is substantial, it will yield a discernible change in electrical conductivity, substantiating the material's high sensitivity to gas molecules.

Figure 9 illustrates the band structures of the Ni-InSe monolayer upon the adsorption of various toxic gases. It is evident that the adsorption of CO, NO, and SO_2 causes the bandgap of the Ni-InSe monolayer to vary from 1.196 eV to 1.419 eV, 1.323 eV, and 1.332 eV, respectively. The extent of change in the bandgap follows the order, CO (18.65%) > SO_2 (11.37%) > NO (10.62%), indicating that the Ni-InSe monolayer is highly sensitive to these three gases. In contrast, the bandgap diminishes to 0.816 eV, 1.142 eV, and 1.190 eV for the adsorption of NO_2, NH_3, and H_2S, respectively. It is apparent that the NH_3/Ni-InSe and H_2S/Ni-InSe systems demonstrate minimal rates of change in the bandgap, with respective values of −4.52% and −0.50%. Nevertheless, the Ni-InSe monolayer displays the highest sensitivity towards NO_2 due to the most substantial rate of change in the bandgap (−31.77%). Consequently, it can be concluded that the Ni-InSe-based gas sensor exhibits a superior sensitivity toward CO, SO_2, NO, and NO_2. In addition, the work function (Φ) can also serve as an evaluative measure of the gas sensor sensitivity, which is defined as

follows [44]: $\Phi = E_{\text{vac}} - E_{\text{fer}}$, where E_{vac} and E_{fer} are the vacuum level and Fermi level of a system, respectively. The work functions of the pristine Ni-InSe monolayer and various adsorption systems are presented in Figure 10. It is observable that the adsorption of NH$_3$ and H$_2$S results in a reduction in the bandgap of Ni-InSe, while the adsorption of other gases leads to an increase in the bandgap of Ni-InSe. The rate of change in the work function follows the sequence, SO$_2$ (11.29%) > NH$_3$ (-8.72%) >CO (6.67%) > NO (5.13%) > H$_2$S (-4.61%) > SO$_2$ (1.03%), suggesting that the Ni-InSe monolayer can function as an Φ-type gas sensor for SO$_2$, NH$_3$, and CO.
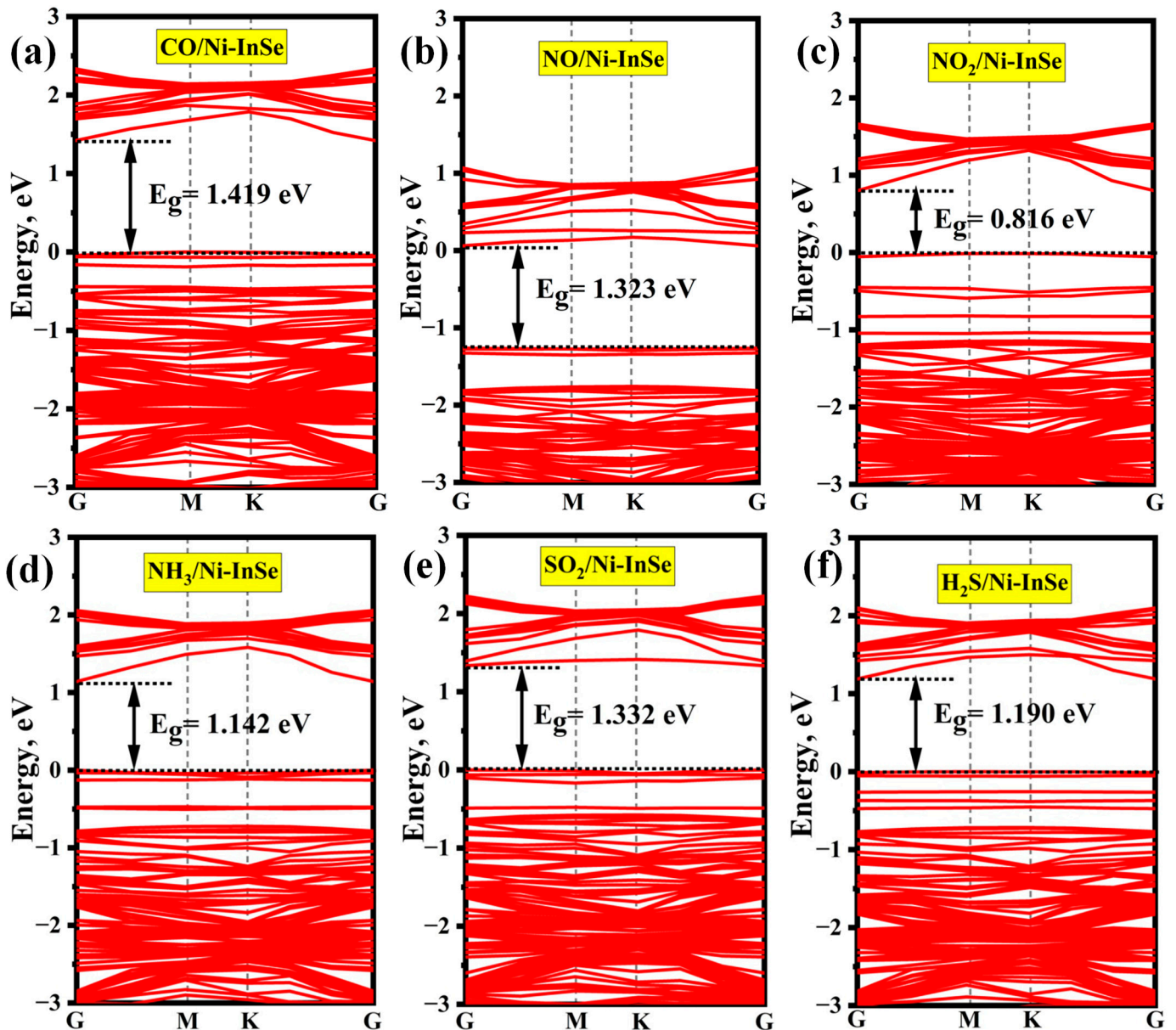

Figure 9. Band structures of different adsorption systems: (**a**) CO/Ni-InSe, (**b**) NO/Ni-InSe, (**c**) NO$_2$/Ni-InSe, (**d**) NH$_3$/Ni-InSe, (**e**) SO$_2$/Ni-InSe, and (**f**) H$_2$S/Ni-InSe.
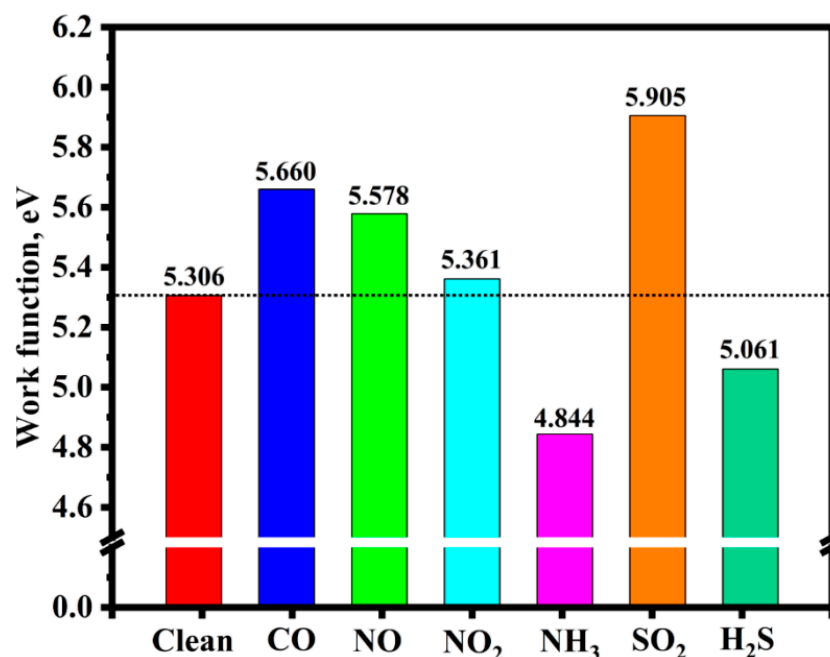
Figure 10. Work functions of the clean Ni-InSe monolayer and different adsorption systems.

Generally, a favorable recovery characteristic is essential for gas sensors with high performance. In simulation calculations, the recovery process is considered as the reverse process of adsorption. According to the transition state theory and the Van't Hoff Arrhenius expression, the recovery time (τ) can be calculated using the following equation [45]:

$$\tau = v_0^{-1}\exp\left(\frac{-E_{ads}}{K_B T}\right) \tag{5}$$

where v_0 is the attempt frequency (10^{12} s^{-1}), K_B is the Boltzmann constant (8.62×10^{-5} eV/K), T is the work temperature (K), and E_{ads} is the adsorption energy of the system. The higher adsorption energy signifies a greater barrier for the desorption process. Consequently, the desorption process becomes more challenging, leading to an extended desorption time. Figure 11 gives the calculated recovery times of various adsorption systems at temperatures of 298 K, 348 K, and 398 K. It is evident that the recovery times for CO, NO, NO$_2$, and NH$_3$ at room temperature are excessively lengthy, ranging from 7.80×10^3 to 6.67×10^{10} s. Even at an elevated temperature of 398 K, the recovery times for CO and NO remain prolonged, hindering the timely release of the adsorbed CO and NO from the Ni-InSe surface. Conversely, NO$_2$ and NH$_3$ exhibit satisfactory recovery times of 0.79 s and 1.06 s at 398 K, suggesting that Ni-InSe can be effectively employed as a recyclable sensing material for NO$_2$ and NH$_3$ at high temperatures. In contrast, the adsorption of SO$_2$ on the Ni-InSe monolayer exhibits a moderate recovery time of 3.24 s at 298 K. This desorption rate is adequate for gas sensor applications; hence, the Ni-InSe-based gas sensors exhibit substantial reusability for the detection of SO$_2$ at room temperature.

The comparative sensing abilities of the Ni-InSe monolayer are contrasted with those of other two-dimensional materials, as listed in Table 2. It is evident that both the Janus Te$_2$Se and C$_3$N monolayers demonstrate weak adsorption capacities and poor sensitivity towards SO$_2$, resulting in notably brief recovery times of 2.66×10^{-6} s and 7.47×10^{-4} s, respectively. This indicates a limited response capability towards the SO$_2$ molecule for these materials. Conversely, materials such as the Sc-MoS$_2$, Zn–MoSe$_2$, Pd$_3$–PtSe$_2$, and Pd-MoTe$_2$ monolayers exhibit significantly stronger adsorption capacities, with E_{ads} values ranging from -1.03 eV to -3.54 eV, thereby leading to prolonged recovery times at 298 K and making the desorption of SO$_2$ challenging. Furthermore, their sensitivity, as evaluated by ΔE_g and $\Delta \Phi$, is noticeably lower compared to that of the Ni-InSe monolayer,

except in the case of Sc-MoS$_2$. Meanwhile, the Ni-InSe monolayer displays a favorable affinity and recovery time towards the SO$_2$ molecule. Consequently, the Ni-InSe monolayer holds substantial promise as a promising sensing material for the detection of SO$_2$ at room temperature.
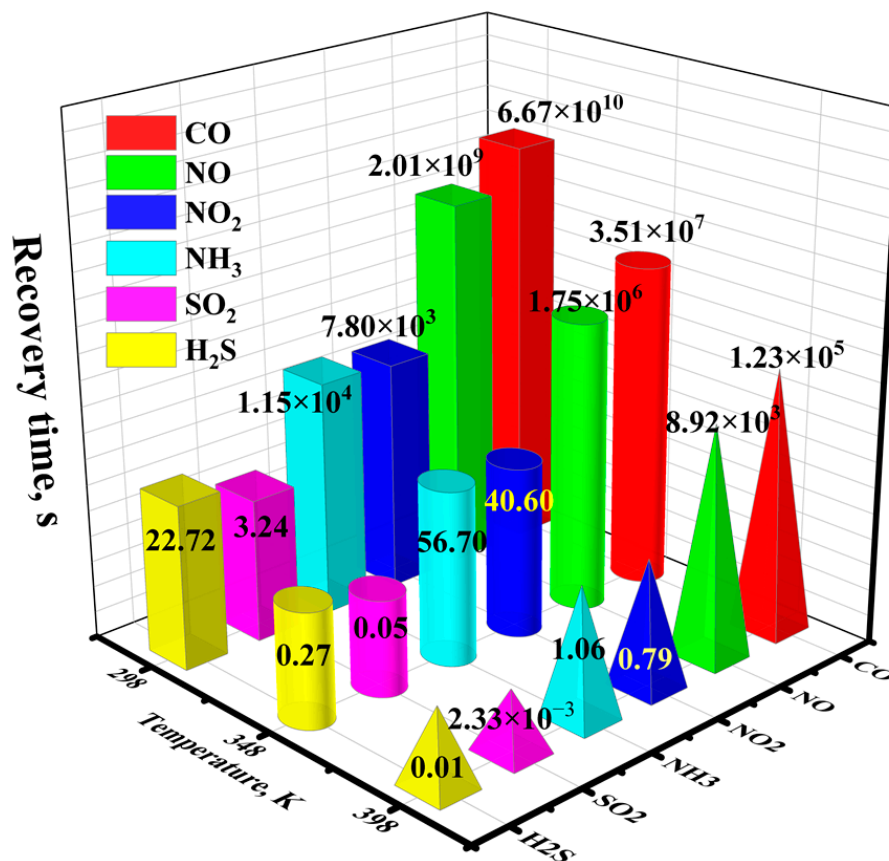

Figure 11. Recovery time (τ) of different toxic gases desorbing from the Ni-InSe monolayer at various temperatures.

Table 2. Comparison of adsorption and sensing properties of different 2D materials towards the SO$_2$ molecule.

Target Gases	Sensing Materials	E_{ads}, eV	ΔE_g, %	$\Delta \Phi$, %	τ, s (298 K)	Ref.
SO$_2$	Sc-MoS$_2$	−3.21	−71.4	/	1.87×10^{42}	[46]
	Janus Te$_2$Se	−0.38	−0.05	/	2.66×10^{-6}	[47]
	Zn–MoSe$_2$	−1.03	3.68		2.59×10^{5}	[48]
	Pd$_3$–PtSe$_2$	−3.54	2.96	3.94	7.08×10^{47}	[49]
	Pd-MoTe$_2$	−1.32	−6.18	/	2.07×10^{10}	[50]
	C$_3$N monolayer	−0.58	0.00	/	7.47×10^{-4}	[51]
	Ni-InSe	−0.74	11.37	11.29	3.24	This work

4. Conclusions

In this work, the first-principles calculations are employed to investigate the adsorption characteristics and electronic properties of twelve different gases on the Ni-InSe monolayer, and their adsorption energy, electronic structure, work function, and recovery time are systematically analyzed. The studied results indicate that Ni doping enhances the electrical conductivity of the InSe monolayer and strengthens the adsorption capabilities for six toxic gases (CO, NO, NO$_2$, NH$_3$, SO$_2$, and H$_2$S). Furthermore, analyses of both TED and CDD plots demonstrate that these toxic gases interact robustly with Ni-InSe through chemical adsorption. Notably, these gases can be effectively distinguished in the presence

of H_2O, CO_2, CH_4, H_2, O_2, and N_2 in the atmosphere. Additionally, the adsorption of CO, NO, NO_2, and SO_2 results in significant alterations to the bandgap of Ni-InSe, with changes of 18.65%, 11.37%, 10.62%, and -31.77%, respectively. Moreover, the analyses of recovery times shows that the SO_2 on the Ni-InSe monolayer exhibit a moderate recovery time of 3.24 s at 298 K, while the NO_2 and NH_3 demonstrate satisfactory recovery times of 0.79 s and 1.06 s at 398 K. Consequently, Ni-InSe is positioned as a promising gas sensor for detecting SO_2 at room temperature and for identifying NO_2 and NH_3 at high temperatures. This work not only provides a theoretical foundation for the potential applications of Ni-InSe-based gas sensors in various industries, such as industrial safety, environmental monitoring, and medical diagnosis, but also bridges the gap between our theoretical study and practical experimental implementation, including the low-cost development, scalability, and integration with existing sensor technologies.

Institutional Review Board Statement: Not applicable.

Informed Consent Statement: Not applicable.

Data Availability Statement: The data will be made available upon request.

Conflicts of Interest: The authors declare no conflicts of interest.

References

1. Nguyet, T.T.; Hung, C.M.; Hong, H.S.; Thai, N.X.; Thang, P.V.; Xuan, C.T.; Van Duy, N.; Theu, L.T.; Van An, D.; Nguyen, H.; et al. Enhanced response characteristics of NO_2 gas sensor based on ultrathin SnS_2 nanoplates: Experimental and DFT study. *Sens. Actuators A Phys.* **2024**, *373*, 115384. [CrossRef]
2. Ma, Y.; Yang, M.; Deng, G.; Xiong, H. Theoretical insights into gas-sensitive properties of B, Ga and In doped WS_2 monolayer towards oxygen-containing toxic gases. *Appl. Surf. Sci.* **2024**, *670*, 160725–160740. [CrossRef]
3. Dolmaseven, S.; Yuksel, N.; Fellah, M. Au, Ag and Cu Doped BNNT for ethylene oxide gas detection: A density functional theory study. *Sens. Actuators A Phys.* **2023**, *350*, 114109. [CrossRef]
4. Gao, X.; Zhou, Q.; Wang, J.; Xu, L.; Zeng, W. Performance of intrinsic and modified graphene for the adsorption of H_2S and CH_4: A DFT study. *Nanomaterials* **2020**, *10*, 299. [CrossRef] [PubMed]
5. Norouzzadeh, E.; Mohammadi, S.; Moradinasab, M. First principles characterization of defect-free and vacancy-defected monolayer $PtSe_2$ gas sensors. *Sens. Actuators A Phys.* **2020**, *313*, 112209. [CrossRef]
6. Tang, H.; Sacco, L.N.; Vollebregt, S.; Ye, H.; Fan, X.; Zhang, G. Recent advances in 2D/nanostructured metal sulfide-based gas sensors: Mechanisms, applications, and perspectives. *J. Mater. Chem. A* **2020**, *8*, 24943–24976. [CrossRef]
7. Zeng, J.; Xu, L.; Luo, X.; Chen, T.; Tang, S.-H.; Huang, X.; Wang, L.-L. Z-scheme systems of ASi2N4 (A = Mo or W) for photocatalytic water splitting and nanogenerators. *Tungsten* **2022**, *4*, 52–59. [CrossRef]
8. Yao, Q.; Ren, G.; Xu, K.; Zhu, L.; Khan, H.; Mohiuddin, M.; Khan, M.W.; Zhang, B.Y.; Jannat, A.; Haque, F.; et al. 2D Plasmonic Tungsten Oxide Enabled Ultrasensitive Fiber Optics Gas Sensor. *Adv. Opt. Mater.* **2019**, *7*, 1901383–1901391. [CrossRef]
9. Ma, Y.; Deng, G.; Xiong, H. Density function theory investigation of bimetallic phthalocyanine as a potential sensor and scavenger for nitrogen-containing toxic gases. *J. Environ. Chem. Eng.* **2024**, *12*, 113687. [CrossRef]
10. Dong, X.; Peng, Z.; Chen, T.; Xu, L.; Ma, Z.; Liu, G.; Cen, K.; Xu, Z.; Zhou, G. Electronic structures and transport properties of low-dimensional GaN nanoderivatives: A first-principles study. *Appl. Surf. Sci.* **2021**, *561*, 150038–150045. [CrossRef]
11. Yang, F.; Hu, P.; Hua, X.-J.; Chen, B.; Gao, L.; Wang, K.-S. Photocatalytic applications and modification methods of two-dimensional nanomaterials: A review. *Tungsten* **2024**, *6*, 77–113. [CrossRef]

12. Wang, J.-H.; Yang, S.-W.; Ma, F.-B.; Zhao, Y.-K.; Zhao, S.-N.; Xiong, Z.-Y.; Cai, D.; Shen, H.-D.; Zhu, K.; Zhang, Q.-Y.; et al. RuCo alloy nanoparticles embedded within N-doped porous two-dimensional carbon nanosheets: A high-performance hydrogen evolution reaction catalyst. *Tungsten* **2023**, *6*, 114–123. [CrossRef]

13. Liu, G.; Chen, T.; Dong, X.; Huang, L.; Xu, Z.; Xiao, X. High gas sensing performance of inorganic and organic molecule sensing devices based on the BC_3N_2 monolayer. *Phys. Chem. Chem. Phys.* **2023**, *24*, 23769–23778. [CrossRef] [PubMed]

14. Cai, Y.; Zhang, G.; Zhang, Y.-W. Charge Transfer and Functionalization of Monolayer InSe by Physisorption of Small Molecules for Gas Sensing. *J. Phys. Chem. C* **2017**, *121*, 10182–10193. [CrossRef]

15. Chen, D.; Zhang, X.; Cui, H.; Tang, J.; Pi, S.; Cui, Z.; Li, Y.; Zhang, Y. High selectivity n-type InSe monolayer toward decomposition products of sulfur hexafluoride: A density functional theory study. *Appl. Surf. Sci.* **2019**, *479*, 852–862. [CrossRef]

16. Zheng, W.; Yang, C.; Li, Z.; Xie, J.; Lou, C.; Lei, G.; Liu, X.; Zhang, J. Indium selenide nanosheets for photoelectrical NO_2 sensor with ultra sensitivity and full recovery at room temperature. *Sens. Actuators B Chem.* **2021**, *329*, 129127–129136. [CrossRef]

17. Dong, X.; Chen, T.; Zhou, G. Design high performance field-effect, strain/gas sensors of novel 2D penta-like Pd_2P_2SeX (X=O, S, Te) pin-junction nanodevices: A study of transport properties. *J. Alloys Compd.* **2024**, *977*, 173417. [CrossRef]

18. Ma, D.; Ju, W.; Tang, Y.; Chen, Y. First-principles study of the small molecule adsorption on the InSe monolayer. *Appl. Surf. Sci.* **2017**, *426*, 244–252. [CrossRef]

19. Yang, M.; Xiong, H.; Ma, Y.; Yang, L. Theoretical investigation of Ag and Au modified CSiN monolayer as a potential gas sensor for air decomposition components detection. *J. Mol. Liq.* **2024**, *410*, 125648. [CrossRef]

20. Junkaew, A.; Arróyave, R. Enhancement of the selectivity of MXenes (M2C, M = Ti, V, Nb, Mo) via oxygen-functionalization: Promising materials for gas-sensing and -separation. *Phys. Chem. Chem. Phys.* **2018**, *20*, 6073–6082. [CrossRef]

21. Ma, D.; Li, T.; Yuan, D.; He, C.; Lu, Z.; Lu, Z.; Yang, Z.; Wang, Y. The role of the intrinsic Se and In vacancies in the interaction of O_2 and H_2O molecules with the InSe monolayer. *Appl. Surf. Sci.* **2018**, *434*, 215–227. [CrossRef]

22. Liu, G.; Chen, T.; Zhou, G.; Xu, Z.; Xiao, X. Nonvolatile Electrical Control and Reversible Gas Capture by Ferroelectric Polarization Switching in 2D FeI_2/In_2S_3 van der Waals Heterostructures. *ACS Sens.* **2023**, *8*, 1440–1449. [CrossRef] [PubMed]

23. Dong, X.; Chen, T.; Liu, G.; Xie, L.; Zhou, G.; Long, M. Multifunctional 2D g-C_4N_3/MoS_2 vdW Heterostructure-Based Nanodevices: Spin Filtering and Gas Sensing Properties. *ACS Sens.* **2022**, *7*, 3450–3460. [CrossRef] [PubMed]

24. Lu, D.; Huang, L.; Zhang, J.; Zhang, Y.; Feng, W.; Zeng, W.; Zhou, Q. Rh- and Ru-Modified InSe Monolayers for Detection of NH_3, NO_2, and SO_2 in Agricultural Greenhouse: A DFT Study. *ACS Appl. Nano Mater.* **2023**, *6*, 14447–14458. [CrossRef]

25. Cheng, W.; Ni, J. CO_2 gas sensor based on Pt-, Ag-, Au- and Pd-doped InSe monolayer: A first-principles study. *Semicond. Sci. Technol.* **2022**, *37*, 095011–095020. [CrossRef]

26. Yan, Y.; Luo, Y.; Li, Y.; Zhang, Y.; Wu, P.; Tang, J.; Zhang, X.; Xiao, S. Transition metal (Au, Ag, Pt, Pd, Ni) doped MoS_2 as gas sensing materials for C_4F_7N leakage detection: A comparative study. *Surf. Interfaces* **2023**, *44*, 103625–103934. [CrossRef]

27. Zhang, B.; Liu, K.; Xie, K.; Wang, P.; Lin, L.; Su, L. Adsorption of toxic and harmful gas NO_2 and SO_2 on TM (Fe, Co and Ni) modified $ZrSe_2$ monolayer: A DFT study. *Mater. Today Commun.* **2024**, *39*, 108483. [CrossRef]

28. Lu, D.; Huang, L.; Zhang, J.; Zeng, W.; Zhou, Q. Density Functional Theory Investigation of Pristine and Ni-Doped CeO_2 (110) for C_2H_4 Detection Based on Optimized Work Functions. *ACS Appl. Nano Mater.* **2024**, *7*, 4239–4251. [CrossRef]

29. Zhang, J.; Li, T.; Zhang, H.; Huang, Z.; Zeng, W.; Zhou, Q. Ni decorated ReS_2 monolayer as gas sensor or adsorbent for agricultural greenhouse gases NH_3, NO_2 and Cl_2: A DFT study. *Mater. Today Chem.* **2024**, *38*, 102114. [CrossRef]

30. Delley, B. From molecules to solids with the $DMol^3$ approach. *J. Chem. Phys.* **2000**, *113*, 7756–7764. [CrossRef]

31. Grimme, S. Semiempirical GGA-type density functional constructed with a long-range dispersion correction. *J. Comput. Chem.* **2006**, *27*, 1787–1799. [CrossRef] [PubMed]

32. Inada, Y.; Orita, H. Efficiency of numerical basis sets for predicting the binding energies of hydrogen bonded complexes: Evidence of small basis set superposition error compared to Gaussian basis sets. *J. Comput. Chem.* **2008**, *29*, 225–232. [CrossRef] [PubMed]

33. Chen, J.; Jia, L.; Cui, X.; Zeng, W.; Zhou, Q. Adsorption and gas-sensing properties of SF6 decomposition components (SO_2, SOF_2 and SO_2F_2) on Co or Cr modified GeSe monolayer: A DFT study. *Mater. Today Chem.* **2023**, *28*, 101382–101395. [CrossRef]

34. Monkhorst, H.J.; Pack, J.D. Special points for Brillouin-zone integrations. *Phys. Rev. B* **1976**, *13*, 5188–5192. [CrossRef]

35. Zhang, H.; Zhou, W.; Jiang, J.; Zeng, W.; Zhou, Q. First-Principles Investigation of Transition Metal (Co, Rh, and Ir)-Modified WS2 Monolayer Membranes: Adsorption and Detection of SF6 Decomposition Gases. *ACS Appl. Nano Mater.* **2024**, *7*, 13379–13391. [CrossRef]

36. Ma, Y.; Xiong, H.; Zhang, J. Proposals for gas-detection improvement of the FeMPc monolayer towards ethylene and formaldehyde by using bimetallic synergy. *Phys. Chem. Chem. Phys.* **2024**, *26*, 12070–12083. [CrossRef]

37. Wang, M.; Cao, J.; Zhang, Y.; Liu, J.; Chen, D.; Jia, P. Crn (n = 1–4) clustered (8, 0) single-walled CNT: Comparison of gas-sensitive properties to air discharge pollutants (CO, NO_x). *Surf. Interfaces* **2023**, *44*, 103619. [CrossRef]

38. Qian, G.; Peng, Q.; Zou, D.; Wang, S.; Yan, B.; Zhou, Q. First-Principles Insight Into Au-Doped MoS_2 for Sensing C_2H_6 and C_2H_4. *Front. Mater.* **2020**, *7*, 1–9. [CrossRef]

39. Ju, W.; Li, T.; Zhou, Q.; Li, H.; Li, X.; Ma, D. Adsorption of 3d transition-metal atom on InSe monolayer: A first-principles study. *Comput. Mater. Sci.* **2018**, *150*, 33–41. [CrossRef]

40. Brotons-Gisbert, M.; Andres-Penares, D.; Suh, J.; Hidalgo, F.; Abargues, R.; Rodríguez-Cantó, P.J.; Segura, A.; Cros, A.; Tobias, G.; Canadell, E.; et al. Nanotexturing To Enhance Photoluminescent Response of Atomically Thin Indium Selenide with Highly Tunable Band Gap. *Nano Lett.* **2016**, *16*, 3221–3229. [CrossRef]

41. Qiu, X.; Xu, D.; Li, Z.; Dong, J.; Hou, D.; Xiong, H. Atomic-level insights into sensing performance of toxic gases on the InSe monolayer decorated with Pd and Pt under humid environment. *Sens. Actuators A Phys.* **2024**, *378*, 115846. [CrossRef]
42. Zhang, H.; Ma, Y.; Xiong, H.; Deng, G.; Yang, L.; Nie, Z. Highly sensitive and selective sensing-performance of 2D Co-decorated phthalocyanine toward NH_3, SO_2, H_2S and CO molecules. *Surf. Interfaces* **2023**, *36*, 102641–102653. [CrossRef]
43. Hou, T.; Zeng, W.; Zhou, Q. Pd-GaSe and Pd_3-GaSe Monolayers: Two Promising Candidates for Detecting Dissolved Gases in Transformer Oil. *Chemosensors* **2022**, *10*, 236. [CrossRef]
44. Lin, L.; Feng, Z.; Dong, Z.; Tao, H.; Hu, C. Transition metal disulfide ($MoTe_2$, $MoSe_2$ and MoS_2) were modified to improve NO_2 gas sensitivity sensing. *J. Ind. Eng. Chem.* **2023**, *118*, 533–543. [CrossRef]
45. Naseem, N.; Tariq, F.; Malik, Y.; Zahid, W.A.; El-Fattah, A.A.; Ayub, K.; Iqbal, J. Sensing ability of carbon nitride (C_6N_8) for the detection of carbon monoxide (CO) and carbon dioxide (CO_2). *Sens. Actuators A Phys.* **2023**, *366*, 114947. [CrossRef]
46. Li, B.; Zhou, Q.; Peng, R.; Liao, Y.; Zeng, W. Adsorption of SF6 decomposition gases (H_2S, SO_2, SOF_2 and SO_2F_2) on Sc-doped MoS_2 surface: A DFT study. *Appl. Surf. Sci.* **2021**, *549*, 149271. [CrossRef]
47. Zhu, B.; Zheng, K.; Chen, X.; Qiu, J.; Guo, H.; Zhang, F.; Lang, L.; Yu, J.; Bao, J. Monolayer Janus Te_2Se-based gas sensor to detect SO_2 and NOx: A first-principles study. *Phys. Chem. Chem. Phys.* **2021**, *23*, 1675–1683. [CrossRef]
48. Ayesh, A.I. DFT investigation of H_2S and SO_2 adsorption on Zn modified $MoSe_2$. *Superlattices Microstruct.* **2021**, *162*, 107098. [CrossRef]
49. Li, M.; Cen, W.; Tian, Z.; Zheng, Q. First Principles Calculation of Gas Sensitive Properties of Pd3-Modified Monolayer $PtSe_2$ to SF_6 Decomposition Products. *Phys. Status Solidi* **2024**, *18*, 2300367–2300377. [CrossRef]
50. Huang, F.; Sang, T.-Y.; Hu, X.; Wang, Z.; Chen, W. Adsorption behaviors and electronic properties of Pd-doped $MoTe_2$ monolayer for hazardous gases detecting and scavenging. *Mater. Sci. Semicond. Process.* **2023**, *170*, 107920. [CrossRef]
51. Xiong, H.; Zhang, H.; Gan, L. A new bifunctional C_3N nanosheet of NO_2, SO_2 gas sensor and CO_2 separation: A first-principles study. *Phys. E Low-Dimens. Syst. Nanostruct.* **2020**, *126*, 114463–114470. [CrossRef]